

Electroencephalogram-based Multi-class Decoding of Attended Speaker's Direction with Audio Spatial Spectrum

Yuanming Zhang, *Student Member, IEEE*, Jing Lu, *Member, IEEE*, Zhibin Lin, Fei Chen, *Senior Member IEEE*, Haoliang Du, Xia Gao

Abstract—Decoding the directional focus of an attended speaker from listeners' electroencephalogram (EEG) signals is essential for developing brain-computer interfaces to improve the quality of life for individuals with hearing impairment. Previous works have concentrated on binary directional focus decoding, i.e., determining whether the attended speaker is on the left or right side of the listener. However, a more precise decoding of the exact direction of the attended speaker is necessary for effective speech processing. Additionally, audio spatial information has not been effectively leveraged, resulting in suboptimal decoding results. In this paper, we observe that, on our recently presented dataset with 15-class directional focus, models relying exclusively on EEG inputs exhibits significantly lower accuracy when decoding the directional focus in both *leave-one-subject-out* and *leave-one-trial-out* scenarios. By integrating audio spatial spectra with EEG features, the decoding accuracy can be effectively improved. We employ the CNN, LSM-CNN, and EEG-Deformer models to decode the directional focus from listeners' EEG signals with the auxiliary audio spatial spectra. The proposed Sp-Aux-Deformer model achieves notable 15-class decoding accuracies of 57.48% and 61.83% in *leave-one-subject-out* and *leave-one-trial-out* scenarios, respectively.

Index Terms—Auditory Attention Decoding, Deep Neural Network, Directional Focus Decoding, Sound Source Localization, Electroencephalogram

I. Introduction

The human brain can extract the speech of the attended speaker amidst competing speakers and environmental noise [1], [2]. However, individuals with hearing impairments often struggle to understand speech, especially in noisy environments, necessitating the use of hearing aids [3], [4].

Modern hearing aids typically assume that the attended speaker is either the one producing the highest sound pressure level or the one located directly in front of the listener [5], [6]. However, these assumptions may not hold in practice, as the desired speaker could be masked by interference or positioned significantly away from the listener. Determining the direction of the attended speaker from interfering speakers using only the signals captured by the hearing aids' microphones is infeasible without prior information, such as the pre-recorded speech of the attended speaker. Recent advancements in auditory attention decoding (AAD) [7], [8] have introduced a viable approach to decode the direction of the attended speaker directly from brain signals, with electroencephalogram (EEG) being the most commonly used technique due to its non-invasive and convenient capture process [9], [10], [11], [12], [13], [14], [15].

The intricate nonlinear relationship between EEG signals and the attended audio poses a significant challenge for existing directional focus decoding methods. Rule-based methods, such as the filter bank common spatial patterns filter (FB-CSP) [16] and the Riemannian geometry-based classifier (RGC) [8], rely on second-order statistics to decode the attended direction. Deep neural network (DNN) approaches employ convolutional [7], recurrent [17], and self-attention [18] structures to directly extract the attended direction from EEG signals. The FB-CSP utilizes optimized filters to maximize the energy contrast of filtered signals between various directional focus classes [16]. The symmetric positive definite property enables the RGC to decode attended directions from the covariance matrices of EEG signals based on Riemannian distance [8]. These rule-based methods perform well with long EEG segments but degrade with shorter decision windows. A convolutional neural

This work was supported by National Science Foundation of China with (Grant No. 12274221) and Postgraduate Research & Practice Innovation Program of Jiangsu Province (Grant No. KYCX24_0141). (Corresponding author: *Jing Lu*).

Yuanming Zhang and Jing Lu are with Key Lab of Modern Acoustics, Nanjing University, Nanjing 210093, China, and also with the NJU-Horizon Intelligent Audio Lab, Horizon Robotics, Beijing 100094, China (e-mail: yuanming.zhang@smail.nju.edu.cn; lujing@nju.edu.cn).

Zhibin Lin is with Key Lab of Modern Acoustics, Nanjing University, Nanjing 210093, China (e-mail: zblin@nju.edu.cn).

Fei Chen is with the Department of Electrical and Electronic Engineering, Southern University of Science and Technology, Shenzhen 518055, China (e-mail: fchen@sustech.edu.cn).

Haoliang Du and Xia Gao are with the Department of Otolaryngology Head and Neck Surgery, Nanjing Drum Tower Hospital, Jiangsu Provincial Key Medical Discipline (Laboratory), Nanjing University, Nanjing 210008, China (e-mail: haoliangdu@163.com; gaomiaent@163.com).

Color versions of one or more of the figures in this article are available online at <http://ieeexplore.ieee.org>

The EEG recording experiments were approved by the Institutional Review Board of Nanjing Drum Tower Hospital, with ethics approval number: 2022-065-09.

network (CNN) model [7] was proposed to directly extract patterns from EEG signals, achieving superior performance over rule-based methods and demonstrating greater robustness to changes in decision window lengths. The spatial-temporal attention network (STAnet) [18] and the spectro-spatial-temporal convolutional recurrent network (CRN) [17] were developed to further enhance directional focus decoding accuracy. The STAnet dynamically assigns different weights to EEG channels. It employs a convolutional block attention module (CBAM) [19] to differentiate the contribution of different EEG channels, followed by a convolution layer and a multi-head attention (MHA) module [20] to extract temporal features. The CRN incorporates the azimuthal equidistant projection (AEP) method to transform EEG channels from their conventional 1D form into 2D images, facilitating better utilization of EEG sensor information. A convolutional recurrent network (CRN) is then applied to extract patterns in the 3D representation (2 spatial dimensions and 1 temporal dimension) of EEG signals. Recently, we proposed a learnable spatial mapping (LSM) module [21] to convert EEG channels into a 2D form, enhancing the performance of the CNN-based model.

Additionally, various self-attention-based models have been applied to facilitate different BCI tasks due to their high capacity for complex modeling [22], [23], [24], [25], [26], among which the EEG-Deformer [22] has achieved superior classification accuracy in mental tasks, such as cognitive attention, driving fatigue, and cognitive workload detection, with a well-designed structure to capture both coarse- and fine-grained features. The information purification module in EEG-Deformer is also suitable for enhancing directional decoding accuracy.

Existing models predominantly focus on binary directional focus decoding, i.e., determining whether a listener is attending to the left or right side [7], [8], [16], [27]. This limitation significantly hampers the practical application of decoding information, as a more precise angle of the attended speaker becomes crucial for subsequent speech processing. Although there has been research on a four-class directional focus decoding, its performance has not been fully validated in the *leave-one-subject-out* scenario [28].

Although existing models [7], [8], [16], [18], [21], [27] exhibit superior binary decoding accuracy, recent experiment results [29], [30], [31] highlight the significant impact of the cross-validation (CV) paradigm on decoding accuracy. These studies demonstrate that dividing a trial into training, validation, and test sets results in overestimated decoding accuracy, which is uncommon in traditional speech processing datasets.

Recently, an improved CV paradigm, known as *leave-one-out* (LOO-CV), was proposed to evaluate the decoding accuracy of an AAD model [7], [30]. In the LOO-CV paradigm, each trial is exclusively assigned to either the training, validation, or test set, preventing the model from leveraging trial-specific patterns to predict the labels of validation and test trials. Some researchers found that

long-range temporal correlated (LRTC) components in EEG responses contribute to this phenomenon [29], [31], [32], [33], [34], [35]. However, the mechanism behind the long-range temporal correlation is beyond the scope of this paper. Nevertheless, we consider LOO-CV a superior method for evaluating directional focus decoding models, as a BCI device can never capture trials included in its training set.

Decoding multi-class directional cues using only EEG signals remains challenging. However, since BCI devices can easily incorporate both EEG electrodes and microphone units, a practical approach to improve multi-class directional focus decoding is to leverage the spatial cues embedded in audio signals. In this paper, we propose combining the spatial spectrum from multi-channel audio signals with EEG signals to address the directional focus decoding on our recently released 15-class directional attention datasets. Our contributions are highlighted as follows.

- We elaborate on our newly released database, which includes 15 alternative speaker directions and enhances the capability of neural networks to decode the directional focus of attended speakers in a 15-class setting.
- We integrate the spatial spectrum with EEG features using flexible modules in the CNN, LSM-CNN, and EEG-Deformer models.
- We use the EEG-Deformer to decode the attended direction from listeners' EEG signals and compare it with the CNN and LSM-CNN models. We observe that the decoding accuracy of multi-class directional focus decoding is far below our expectation in the LOO-CV test paradigm.
- We train and test our proposed models in challenging *leave-one-trial-out* and *leave-one-subject-out* scenarios. During testing, we make every possible effort to reduce LRTC bias, onset bias, eye movement bias, and other potential biases that may lead to overestimated decoding accuracy.

The remainder of the paper is organized as follows. Section II details our recently released multi-directional auditory attention dataset. Section III introduces the CNN, LSM-CNN, and EEG-Deformer models for decoding 15-class directional focus, including the integration of the LSM module with the CNN model and the structure of the audio-EEG fusion convolution layer. Section IV provides details on training the models. Section V presents the experimental results, comparing our proposed models with existing ones and conducting an ablation study to evaluate the efficacy of spatial-spectrum-fused directional focus decoding in various LOO-CV scenarios. Additionally, we investigate the impact of decision window length and the influence of angle between attended and interfering speakers in Section V.

II. THE NJU AUDITORY ATTENTION DECODING DATASET WITH MULTI-DIRECTIONAL CUES

A. Experiment Setup

EEG preprocessing was performed using the EEGLAB toolbox [42]. The EEG signals were filtered through a bandpass filter between 1 Hz and 32 Hz, consistent with most previous AAD tasks [16], [27], [41]. EEG signals were decomposed

through independent component analysis (ICA), and components containing eye, heart, or muscle artifacts were removed. As instructed by EEGLAB, the EEG signal undergoes interpolation to restore the excluded channels.

C. Audio Signal Preprocessing

Audio recordings with an original sampling rate $f_s = 44.1$ kHz were down-sampled to 8 kHz. The down-sampled audio signals were then transformed into the time-frequency domain via short-time Fourier transform (STFT) with F frequency bins and N time frames, with each time-frequency bin expressed as $Y_l(f, n)$ with l the microphone unit index, f the frequency index, and n the time frame index. Subsequently, the minimum variance distortionless response (MVDR) beamformer [43] was applied to extract the spatial spectrum, which can be represented as

$$P_{mvd} = \frac{1}{F} \sum_{f=0}^{F-1} \frac{1}{\mathbf{g}(f, \theta)^T \mathbf{R}(f)^{-1} \mathbf{g}^*(f, \theta)}, \quad (1)$$

where $\mathbf{g}(f, \theta)$ is the steering vector, $\mathbf{R}(f)$ is the correlation matrix of the microphone array defined as

$$\mathbf{R}(f) = \begin{bmatrix} \mathbf{y}_{1,f}^T \mathbf{y}_{1,f}^* & \mathbf{y}_{1,f}^T \mathbf{y}_{2,f}^* \\ \mathbf{y}_{2,f}^T \mathbf{y}_{1,f}^* & \mathbf{y}_{2,f}^T \mathbf{y}_{2,f}^* \end{bmatrix}, \quad (2)$$

with $\mathbf{y}_{i,f}$ a column vector written as

$$\mathbf{y}_{i,f} = [Y_i(f, 0), Y_i(f, 1), \dots, Y_i(f, N-1)]^T, l = 1, \dots, L. \quad (3)$$

The left microphone unit is designated as the reference point. The angle θ begins at -90° on the left-hand side and extends to 90° on the right-hand side. The steering vector is then simplified to

$$\begin{aligned} \mathbf{g}(f, \theta) &= [g_1(f, \theta), g_2(f, \theta)]^T \\ &= [1, \exp(-2\pi i f \sin(\theta) d / c)]^T. \end{aligned} \quad (4)$$

The first ($l = 1$) and second microphone ($l = 2$) are placed near the left and right ear, respectively.

III. PROPOSED METHODS

A. Overview of Models

Figure 2 depicts the architecture of the models used to decode the direction of attended speakers. Figure 2 (a-1) illustrates the general pipeline of the EEG-based directional focus decoding. A DNN model is trained using EEG signals to predict the most probable direction of the attended speaker. Figure 2 (b-1) presents our proposed audio-EEG directional focus decoding method, in which a spatial spectrum is also provided as the second input of a DNN classifier to boost the directional focus decoding. The remaining sections of Figure 2 detail the structures of the CNN [7], LSM-CNN [21], and EEG-Deformer models (first row) [22], and their variants with a spatial fusion convolution layer (second row), which integrates spatial spectrum information with EEG features to improve decoding accuracy.

Let $\mathcal{X} \in \mathbb{R}^{C \times T}$ be the input EEG with C and T representing the total number of EEG channels and time sample points respectively. The CNN model (Figure 2 (a-2)) directly takes \mathcal{X}

as input and performs convolution along the channel dimension. An average pooling layer condenses the intermediate features, followed by fully connected layers to output the predicted class labels.

Let $\mathbf{p}_s \in \mathbb{R}^{N_l}$ be the spatial spectrum with N_l the number of spatial sampling points of the spectrum. A fusion block is inserted before the convolution block in the Sp-Aux-CNN model (Figure 2 (b-2)) to leverage both EEG and audio spatial information. The fusion block first transforms the spatial spectrum into high-dimensional patterns and then concatenates them with EEG features to form a new tensor. The subsequent convolution block uses the fused tensor as input to determine the attended directions.

Figure 2 (a-3) and (b-3) depict the structure of the proposed LSM-CNN and Sp-Aux-LSM-CNN models, respectively. At the start of the model, a learnable spatial mapping (LSM) module is added, designed to utilize the spatial information of EEG sensors, transforming the EEG channels from 1D into a 2D discretized plane. The output of the LSM module is $\mathcal{Z} \in \mathbb{R}^{C_1 \times C_2 \times T}$, where C_1 and C_2 are the hyperparameters that specify the size of the grids used to describe the target 2D plane. A detailed explanation of the LSM module can be found in the next subsection and our previous research [21], [44]. It is noted that the LSM module leverages the spatial information of EEG electrodes (see Figure 1) but not the spatial information of audio signals, and the Sp-Aux-LSM-CNN model fuses the mapped EEG features with the spatial spectrum instead of the raw EEG signals.

The remaining layers in LSM-CNN resemble those of the conventional network [7], with the only difference being the use of 3D convolution blocks (instead of 2D convolution), followed by an average pooling layer to condense the time dimension. The network uses a flatten layer and Fully Connected (FC) layers to generate the output, which is the attended direction.

The EEG-Deformer model (Figure 2 (a-4)) [22], which demonstrates superior performance in other BCI fields, is a new variant of transformer [20], [23], [24]. We adopted the EEG-Deformer to leverage the audio spatial spectrum by inserting a fusion block after the first EEG encoder. The remainder of Sp-Aux-EEG-Deformer is the same as the original.

B. The Learnable Spatial Mapping Module

Current data-driven methods primarily implement image or speech processing models for directional focus decoding [7], [18]. However, these methods fail to effectively leverage the spatial distribution of EEG electrodes, leading to suboptimal performance. Although EEG sensors (electrodes) are spatially distributed in 3D space, EEG signals are conventionally represented as multi-channel signals with additional descriptive text for each channel. Unfortunately, these texts cannot be directly utilized by DNN models. Therefore, it is crucial to design more effective mechanisms to exploit the spatial distribution of EEG sensors.

An intuitive method for reconstructing spatial information involves transforming the 1D distributed EEG channels onto a 2D uniformly discretized plane based on their original positions. However, our experimental results using this approach exhibited a decline in performance. One potential explanation for this outcome is that the direct mapping significantly deviates from the actual distribution, thereby failing to adequately leverage the available spatial information.

The proposed LSM module is illustrated in Figure 2 (a-3). $C \times 1 \times 1$ convolution filters are applied to process EEG signals \mathcal{X} , and the number of convolution filters equals the number of channels on the 2D plane. These convolution filters have flexible weights updated during backpropagation and are shifted across the temporal dimension to linearly combine all EEG channels, resulting in new virtual channels. The convolution layer contains a total of $C_1 C_2$ kernels, matching the number of virtual channels. Subsequently, a batch normalization layer is applied. The output of the convolution layer can be expressed as

$$\mathcal{Z}(i, t) = \text{BN} \left(\sum_{c=1}^C \mathcal{X}(c, t) \mathcal{G}_i(c) \right) \quad (5)$$

where \mathcal{G}_i is the i -th kernel of the convolution layer in LSM.

The output $\mathcal{Z} \in \mathbb{R}^{C_1 C_2 \times T}$ is an intermediate tensor, which is then rearranged into $\mathcal{Z} \in \mathbb{R}^{C_1 \times C_2 \times T}$ as

$$\mathcal{Z}(c_1, c_2, t) = \mathcal{Z}(c_2 + C_2 \times (c_1 - 1), t) \quad (6)$$

with t the temporal index, c_1 and c_2 the indices of the 2D plane,

respectively.

In addition to incorporating the connectivity between neighboring channels, our proposed LSM module reorganizes the spatial layout of EEG channels. This feature allows subsequent convolution layers to emphasize the intrinsic relationships among channels positioned within the 2D plane. This behavior mimics the simultaneous activation patterns observed in human brains, where neurons tend to activate in conjunction with neighboring neurons [45]. It is important to note that in the context of LSM, the term "spatial" refers to the 2D plane learned by the module, as opposed to the conventional 1D arrangement of EEG recordings.

C. Fusion of spatial spectrum and EEG features

The dotted box in Figure 2 (b-2) depicts the structure of the fusion block, which takes both spatial spectrum and EEG feature as inputs. An FC layer is applied to transform the spatial spectrum into a high-dimensional embedding, which is then reshaped to match the dimensions of the EEG features. The reshaped spatial spectrum embedding is concatenated with the EEG feature to form the output of the fusion block. This approach facilitates the neural network utilizing spatial cues of the competing speakers.

Specifically, let \mathcal{Z} be the intermediate EEG feature, e.g., the output of the LSM module. The fused feature \mathcal{Z} can be represented as

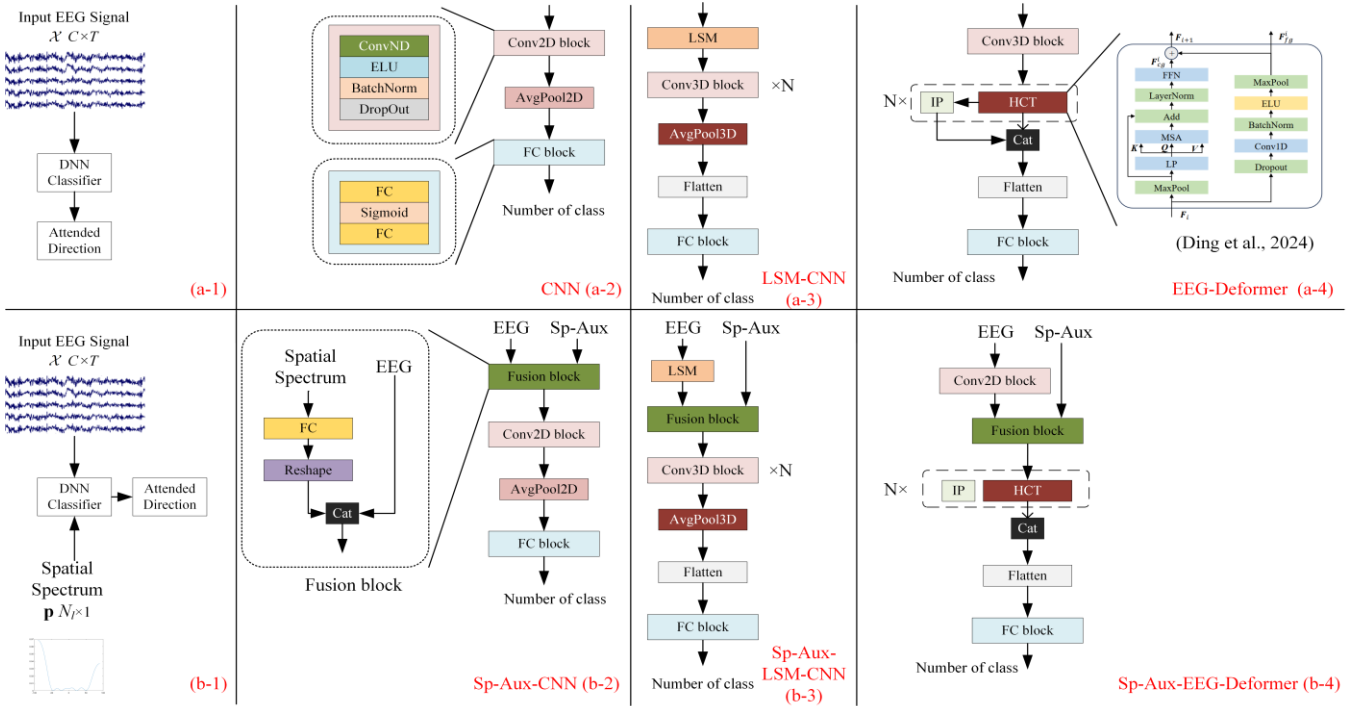


Figure 2 The pipeline of DNN-based multi-class directional focus decoding and the structures of various DNN classifiers. (a/b-1) Pipelines of directional focus decoding with and without spatial information. (a-2~4) Structures of CNN, LSM-CNN, and EEG-Deformer. These models utilize only EEG signals to capture the directions of the attended speakers. (b-2~4) Structures of Sp-Aux-CNN, Sp-Aux-LSM-CNN, and Sp-Aux-EEG-Deformer. These models leverage both EEG signals and spatial information to enhance directional focus decoding performance.

$$\begin{aligned}
\hat{\mathbf{p}}_s &= \text{FC}(\mathbf{p}_s) \\
\mathcal{P} &= \text{reshape}(\mathbf{p}_s, C_1, C_2, 1) \\
\mathcal{Z} &= \text{concat}(\mathcal{Z}, \mathcal{P})
\end{aligned} \tag{7}$$

D. Model performance evaluation

IV. DATA PREPERATION & TRAINING

A. Cross-Validation

It has been revealed that the inherent long-range temporal correlation (LRTC) in EEG signals severely impacts DNN-based directional focus decoding models, resulting in overestimated decoding accuracy [29], [30], [31], [32], [33], [34], [35]. Speaker-related and audio-content-related features may also be captured by DNN models, necessitating carefully designed experiments to mitigate these effects. The participants are required to close their eyes during audio playback to minimize visual bias. However, eye movement components cannot be fully controlled during EEG experiments nor removed by preprocessing algorithms, resulting in unavoidable visual bias.

In our experiments, we made every possible effort to remove

these biases. We demonstrate the employed *LOO* cross-validation paradigms in Figure 3. Figure 3 (a) illustrates the *leave-one-trial-out (LOTO)* scenario, where the training, validation, and test trials never overlap. Additionally, the DNN decoder is trained on the training trials of all subjects and evaluated on the held-out trials of the same subjects. That is to say, the *LOTO* decoder depends on specific subject groups.

Figure 3 (b) depicts the *leave-one-subject-out (LOSO)* scenario. In this scenario, trials from one subject are used to validate and test the models, while trials from other subjects are used to train the DNN decoder. In other words, the DNN decoder never sees any trials from the test subject. Thus, the decoder cannot leverage subject-specific patterns to achieve higher decoding accuracy, making the *leave-one-subject-out* scenario more generalized and more challenging.

Figure 3 (c) demonstrates the *leave-one-moment+trial-out (LOMTO)* condition. In this paradigm, trials adjacent to the validation or test trials (white trials in the figure) are removed. Figure 3 (d) and (e) depict the *leave-one-class+trial-out (LOCTO)* and *leave-one-audio+trial-out (LOATO)* conditions, respectively. The *LOC+TO* datasets follow these rules:

- Trials from one subject may have only one unique class

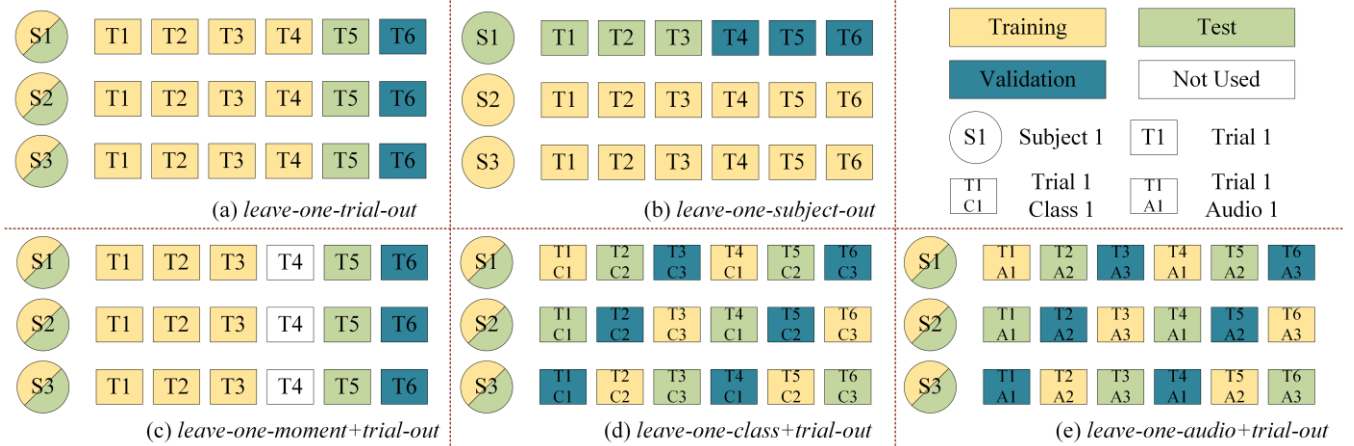


Figure 3 A schematic diagram of the *leave-one-out* cross-validation paradigms. (a) In the *leave-one-trial-out* scenario, some trials are held out to comprise the validation and test sets, and the remaining trials form the training set. (b) In the *leave-one-subject-out* scenario, data from one held-out subject form the validation and test sets, and data from the remaining subjects form the training set. (c) In the *leave-one-moment+trial-out* scenario, the training and evaluation sets consist of nonadjacent trials. (d) In the *leave-one-class+trial-out* scenario, validation and test trials from different subjects have unique class labels. (e) In the *leave-one-audio+trial-out* scenario, validation and test trials from different subjects have unique attended audios. Note that this diagram is for demonstration only, the actual numbers of subjects, trials, classes, and attended audios depend on the dataset.

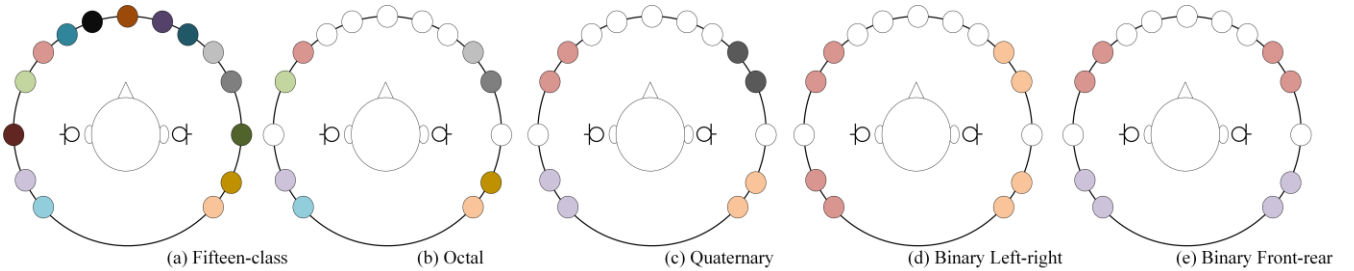


Figure 4 A schematic diagram of the labeling paradigm of our proposed dataset. Various colors indicate various class labels. Non-colored directions are not used.

label. Trials from different subjects must have distinct class labels.

- If a trial is included in one dataset, trials possessing the same class label are also included in that dataset.
- The total number of class labels of one dataset is equal to the number of alternative attention directions, which is 15 in our dataset.

The *LOATO* datasets apply similar restraints to the attended audio:

- Trials from one subject may have only one unique attended audio.
- If a trial is included in one dataset, trials with the same attended audio are also included in that dataset.
- The total number of class labels of one dataset is equal to the number of alternative attention directions, which is 15 in our dataset.

We implement all cross-validation and training procedures using PyTorch [46]. The Adam optimizer is used during the training, and a learning rate drop-down policy is applied to improve convergence. The L2 regularization is applied to further alleviate overfit.

B. Trial Labeling

We demonstrate five distinct trial labeling paradigms in Figure 4. In the first paradigm, all trials are labeled as their directions of attended speakers. In the second paradigm, trials without front-rear counterparts are excluded from the dataset, and the retained trials are labeled as their original attended directions, resulting in eight distinct classes. In the third paradigm, trials retained in the second paradigm are labeled according to the quadrant where they live, leading to a 4-class directional focus decoding dataset. In the last two paradigms, trials are labeled as left-right symmetric (the fourth one) or front-rear symmetric (the fifth one) pairs.

The proposed labeling paradigms facilitate the investigation of impact of number of alternative directions on the performance of directional focus decoding, which is discussed in next section.

C. Spatial Spectrum Computation

The spatial spectrum for each trial was precomputed following Equation (1), and all segments of a single trial were linked to the same spatial spectrum. This method is considered reasonable as it prevents the leakage of trial-specific spatial spectrum patterns into the evaluation sets.

V. RESULTS & DISCUSSION

A. 15-class directional focus decoding accuracy

Table 1 demonstrates the decoding accuracy of the CNN, LSM-CNN, and EEG-Deformer models on our proposed 15-class AAD dataset in the *LOTO* and *LOSO* paradigms with various window lengths. The results indicate that all DNN models cannot decode the attended direction from 15 alternatives using only listeners' EEG signals, and none significantly surpasses the chance level of a 15-class decoder, as shown in Table 1.

However, all models achieve significantly better decoding performance by integrating audio spatial spectra. The simple network structure of the CNN model contributes to its worst decoding accuracy among three spatial-spectrum-informed models. More complicated networks, such as the Sp-Aux-LSM-CNN and Sp-Aux-EEG-Deformer, successfully surpass the chance level of a binary decoder (Wilcoxon sign-rank test, $p < 0.001$), indicating effective fusion of EEG and audio information. Specifically, the Sp-Aux-EEG-Deformer model achieves a decoding accuracy of 61.83% with a decision window length of 10 seconds in the *LOTO* scenario. Notably, the Sp-Aux-EEG-Deformer surpasses the Sp-Aux-LSM-CNN in all scenarios, demonstrating its superior modeling capabilities.

Both Sp-Aux-LSM-CNN and Sp-Aux-EEG-Deformer models attain a higher decoding accuracy on a longer decision window length, which is consistent with previous studies [7], [16], [47]. However, the Sp-Aux-CNN model achieved a deteriorated performance with longer EEG samples. An explanation is that the single-layer structure of the CNN model [7] contributes to a limited temporal receptive field, resulting in degraded feature recognition capability. Due to its performance deterioration, the CNN model is excluded from further analysis.

B. The impact of number of alternative directions

As shown in the first, third, and fifth rows of Table 1, none of the three DNN models surpass the chance level of a 15-class decoder (Wilcoxon sign rank test, $p > 0.05$). In addition to the 15-class labeling paradigm, we propose four paradigms with fewer alternative directions to validate the efficacy of our EEG dataset, as demonstrated in Figure 4. The binary front-rear paradigm is used in the next subsections and is not shown in Table 2.

Table 2 presents the decoding accuracy of EEG-Deformer models and its Sp-Aux variants in the binary (2-class), quaternary (4-class), and octal (8-class) directional focus decoding scenarios. It is shown that EEG-Deformer achieves higher decoding accuracies as the number of alternative directions decreases. Specifically, the EEG-Deformer model obtains decoding accuracies of 61.82%, 32.39%, and 22.16% in the binary, quaternary, and octal directional focus decoding experiments, respectively. Significant differences between the decoding accuracies of EEG-Deformer and the random guess decoder are found in the 2-class and 4-class decoding scenarios (Wilcoxon sign rank test, $p < 0.05$). Therefore, it is feasible to decode multi-class directional focus solely based on listeners' EEG signals, and the efficacy of our dataset is validated. Additionally, experimental results suggest that auditory-evoked EEG responses contain effective but limited information about the attended direction of the listeners, leading to degraded performance of 8-class and 15-class directional focus decoding.

Experimental results in the last rows of Table 1 and Table 2 suggest that, rather than simply reducing the alternative directions to where competing speakers are present, the fusion of the spatial spectrum and EEG features results in more effective decoding of the attended direction. Specifically, the

Sp-Aux-EEG-Deformer model achieves decoding accuracies of 64.75%, 60.91%, and 62.95% in the binary, quaternary, and octal scenarios. Additionally, the number of alternative directions also negatively impacts the decoding performance of the Sp-Aux-EEG-Deformer model when the spatial spectrum is fused.

C. The impact of spatial spectrum

Although the advantage of fusing audio spatial cues in directional focus decoding has been demonstrated in Table 1 and Table 3, we will further discuss the impact of spatial spectrum fusion to provide extra insight into the fusion of spatial spectrum and EEG signals.

As depicted in Table 1 and Table 3, both Sp-Aux-LSM-CNN and Sp-Aux-EEG-Deformer models achieve significantly higher decoding accuracy by integrating the audio spatial spectrum and EEG features. Additionally, they achieve decoding accuracy above the chance level of a binary decoder, suggesting the effective integration and utilization of both features, as relying solely on audio features results in a binary random guess decoder.

The microphone array used in our experiment contains two units, one placed near the left ear and another near the right ear. Traditionally, a two-element microphone array cannot distinguish whether the sound source is coming from the front or rear. And our dataset includes some attended directions that are front-rear symmetric, such as 60° versus 120° , and -45° versus -135° . However, an array placed near the head provides not only the left/right spatial cues but also informs the DNN model of the front/rear information. (If not, the DNN model tends to become a four-class random guess decoder.) A convincing explanation is that listeners' heads affect the time delay of audio signals, resulting in divergent spatial spectra between front-incident and rear-incident audio waves. This variance is then recognized by the DNN model and reflected in the contrasting audio spatial features.

As depicted in Figure 4, we retain only $\pm 135^\circ$, $\pm 120^\circ$, $\pm 60^\circ$, and $\pm 45^\circ$ in the dataset and train DNN models on it to validate their capability to decode front-rear spatial cues. The proposed Sp-Aux-EEG-Deformer achieves a decoding accuracy of 62.95% with a standard deviation of 4.23% in the octal front-rear-symmetric dataset, exhibiting a strong capability to

Table 1 Decoding accuracy of CNN, LSM-CNN, and EEG-Deformer models in the LOSO and LOTO scenarios. The “Sp-Aux” denotes a spatial-spectrum-auxiliary DNN model, leveraging spatial cues from the input spatial spectrum, whereas other models rely solely on listeners' EEG signals to decode the attended direction. Asterisk (*) indicates the significant level of Wilcoxon sign rank test against a binary random guess decoder.

Model	CV paradigm	LOSO		LOTO	
	Sample length	1 second	10 seconds	1 second	10 seconds
CNN	-	9.83% \pm 2.56%	10.42% \pm 3.54%	7.18% \pm 0.59%	9.17% \pm 2.82%
	Sp-Aux	50.49% \pm 4.09%	48.62% \pm 6.45%	49.87% \pm 7.13%	39.49% \pm 10.88%
LSM-CNN	-	8.88% \pm 2.46%	10.57% \pm 2.95%	7.64% \pm 1.84%	7.75% \pm 1.16%
	Sp-Aux	55.44%\pm2.29%*	56.11%\pm2.25%*	58.38%\pm3.61%*	61.40%\pm1.35%***
EEG-Deformer	-	9.00% \pm 2.45%	8.92% \pm 2.26%	8.40% \pm 1.74%	9.94% \pm 2.51%
	Sp-Aux	57.48%\pm2.13%***	56.32%\pm0.96%***	60.01%\pm1.72%***	61.83%\pm2.53%***

Table 2 Decoding accuracy and standard deviation of EEG-Deformer and Sp-Aux-EEG-Deformer in the LOSO and LOTO scenarios with various number of alternative directions. The decision window length is 10 seconds. Asterisk (*) indicates the significant level of Wilcoxon sign rank test against a binary random guess decoder.

CV paradigm	Binary Left-Right (2-class)		Quaternary (4-class)		Octal (8-class)	
	LOSO	LOTO	LOSO	LOTO	LOSO	LOTO
EEG-Deformer	56.55% \pm 2.77%***	61.82% \pm 2.10%***	29.17% \pm 2.59%	32.39% \pm 5.89%***	20.55% \pm 1.04%	22.16% \pm 2.66%
Sp-Aux-EEG-Deformer	64.76%\pm2.24%***	64.75%\pm5.23%***	62.72%\pm2.47%***	60.91%\pm6.52%***	59.96%\pm1.36%***	62.95%\pm4.23%***

Table 3 Decoding accuracy of LSM-CNN and EEG-Deformer models in the LOMT, LOATO, LOCTO scenarios. The “Sp-Aux” denotes a spatial-spectrum-auxiliary DNN model, which leverages the spatial cues from the input spatial spectrum, whereas other models rely solely on listeners' EEG signals to decode the attended direction. Please refer to Figure 3 for a more schematic explanation of the LOO scenarios. Asterisk (*) indicates the significant level of Wilcoxon sign rank test against a binary random guess decoder.

Model	CV paradigm	LOMTO		LOCTO		LOATO	
	Sample length	1 second	10 seconds	1 second	10 seconds	1 second	10 seconds
LSM-CNN	-	6.26% \pm 2.23%	9.04% \pm 1.31%	4.43% \pm 3.32%	6.63% \pm 2.28%	6.01% \pm 0.19%	8.43% \pm 1.63%
	Sp-Aux	57.06%\pm5.20%	59.82%\pm6.74%*	52.21%\pm3.89%	61.59%\pm12.04%*	53.13%\pm0.83%*	54.35%\pm1.32%*
EEG-Deformer	-	8.12% \pm 1.97%	9.52% \pm 0.83%	6.20% \pm 4.72%	6.51% \pm 1.57%	6.57% \pm 0.69%	8.93% \pm 0.50%
	Sp-Aux	57.94%\pm5.18%**	60.26%\pm5.44%**	53.19%\pm5.93%	58.15%\pm5.64%	53.01%\pm0.88%*	55.45%\pm0.49%***

distinguish the spatial cues hidden in the audio spatial spectrum. Result of Wilcoxon sign rank test confirms a significant difference between the 8-class (octal) front-rear-symmetric directional focus decoder and a binary random decoder ($p < 0.001$).

Furthermore, we train a binary directional focus decoder which takes the spatial spectrum as the only input on a front-rear-symmetric binary dataset (Figure 4 e) to test our hypothesis that front-rear spatial cues can be decoded by DNN models. Notably, the spatial spectra in the training set are also absent in the evaluation sets. The Sp-Aux-EEG-Deformer obtains a binary front-rear decoding accuracy of 100%, suggesting the existence of front-rear spatial cues and the utilization of such features by the DNN models.

D. The impact of unseen subject

An ideal auditory BCI device is designed to operate on an unseen user, who is not included in its training set. Additionally, a *LOTO* decoder tends to decode LRTC components in the test trials, resulting in overestimated decoding accuracies [29], [30], [31], making it more valuable to train a directional focus decoder in the *LOSO* scenario. A *LOSO* decoder cannot leverage LRTC components which exist in adjacent trials of the same subject, since the validation and test trials never come from training subjects. (See Figure 3 for a schematic demonstration.)

Extensive experiments confirm the degradation of a 15-class directional focus decoder in the *LOSO* scenario. Table 1 demonstrates the decoding performance of Sp-Aux-LSM-CNN and Sp-Aux-EEG-Deformer models from the joint input of EEG and spatial spectrum, significantly surpassing the chance level of a 15-class and binary decoder. (Wilcoxon sign-rank test, $p < 0.001$) The Sp-Aux-EEG-Deformer achieves the highest *LOSO* decoding accuracy of 57.48% with a decision window length of 1 second. The Sp-Aux-LSM-CNN model also obtains a *LOSO* decoding accuracy of 55.44% with 1-second samples. Slight differences are observed between the *LOSO* decoding accuracies of Sp-Aux-LSM-CNN and Sp-Aux-EEG-Deformer models. Compared to the *LOTO* decoders, the *LOSO* ones achieve degraded performance in the 15-class and 8-class directional focus decoding tasks, which is consistent with previous findings [7], [16]. However, the Sp-Aux-LSM-CNN obtains a higher decoding accuracy in the *LOSO* scenarios than the *LOTO* scenarios.

E. The impact of unseen trials with additional constraints

To the best of our knowledge, previous research has not fully investigated the impact of the *leave-one-trial-out* cross-validation scenario with additional constraint conditions. Therefore, we conduct extensive experiments to find out potential biases. Specifically, we construct three *leave-one-trial-out* datasets with additional various constraints. A schematic description of the three datasets is shown in Figure 3.

As shown in the first two columns of Table 3, the Sp-Aux-LSM-CNN and Sp-Aux-EEG-Deformer models slightly deteriorate on the *LOMTO* dataset. Unlike binary

directional focus decoding, adjacent trials in our 15-class dataset inherently possess distinct attention labels. Therefore, a 15-class decoder cannot leverage LRTC features to achieve higher decoding accuracy in these scenarios.

The *LOCTO* dataset poses a greater challenge for DNN models. The second two columns of Table 3 demonstrate a moderate degradation in the 15-class decoding accuracy of both LSM-CNN and EEG-Deformer models. It is noted that the Sp-Aux-LSM-CNN model obtains higher decoding accuracy on the held-out class dataset with a decision window length of 10 seconds, and the degradation is more severe with a shorter decision window length. The Sp-Aux-EEG-Deformer model also achieves a lower decoding accuracy in the *LOCTO* scenario, and the decoding performance degradation is more significant when the decision window length is set to 1 second.

The *LOCTO* dataset introduces a new limitation for DNN models by excluding trials with the same attended *direction* in the evaluation sets from the training set. Hence, the model cannot utilize features from the same-class training trials to obtain a higher decoding accuracy.

Finally, both models are trained on the *LOATO* dataset. It is shown that both models significantly deteriorate on the *LOATO* dataset. However, they still successfully distinguish the attended direction from the alternatives and surpass the chance level of a binary decoder. This decline is attributed to the unseen attended *audio* in the validation and test sets and suggests a potential overfitting on the audio-dependent features.

In general, new limitations to *leave-one-trial-out* datasets pose significant challenges on DNN models. Nevertheless, we believe it necessary to conduct such experiments to fully evaluate the generalization capability and robustness of a data-driven directional focus decoding model. As our EEG dataset is not designed for these experiment conditions, e.g., unseen attended audio, we cannot construct a *leave-one-audio+subject-out* dataset to evaluate the performance of DNN decoders. Carefully designed EEG datasets are desired to meet the requirements for conducting such experiments.

Overall, the fusion of spatial spectrum and EEG features is an effective step toward multi-class directional focus decoding. DNN models not only rely on EEG signals but also learn to leverage spatial cues embedded in the spatial spectrum to obtain higher decoding accuracy.

VI. CONCLUSIONS

This paper presents our newly recorded NJU auditory attention decoding dataset. To our knowledge, this is the first EEG recording dataset featuring 15 alternative directions for attended speakers. Using this dataset, we validate the feasibility of 15-class decoding of directional focus, which offers more effective information for subsequent speech processing compared to the commonly investigated binary decoding. We propose integrating the spatial spectrum with EEG features to enhance 15-class directional focus decoding. We introduce a

fusion block to combine audio spatial features and EEG features to determine the attended directions. We conducted extensive experiments using the *leave-one-out* cross-validation paradigm, known for its realistic and stringent approach for testing directional focus decoders, to assess the feasibility of our proposed method. Specifically, we found the 15-class decoding accuracy to be quite low, close to the chance level. However, the experimental results show that the proposed Sp-Aux-EEG-Deformer model can achieve up to 61.83% average accuracy, significantly surpassing the CNN baseline. The Sp-Aux-LSM-CNN model also achieves an average decoding accuracy of 58.38%. The Sp-Aux-EEG-Deformer model achieves 15-class decoding accuracy of 57.48% in the *leave-one-subject-out* scenario. Statistical analysis shows a significant difference between the accuracy of the Sp-Aux-LSM-CNN and Sp-Aux-EEG-Deformer models and the chance level of binary classification, indicating that our proposed methods successfully leverage both audio and EEG signals to decode the directions of attended speakers from 15 alternative directions. Furthermore, we demonstrate the robustness of our models in the *leave-one-audio+trial-out*, *leave-one-moment+trial-out*, and the *leave-one-class+trial-out* scenarios. Results indicate severe deterioration when the attended audio is unseen during training. In contrast, the long-range temporal correlated component has little impact on the decoding results, as participants are always required to attend to different directions in adjacent trials. However, the fusion strategy we proposed is suboptimal, and a well-designed DNN model is needed for effective utilization of both audio and EEG features for directional focus decoding. Additionally, the limitation of available EEG data results in significant overfitting of our DNN models, and sufficient data are required to train a DNN model effectively.

REFERENCES

- [1] E. C. Cherry, "Some experiments on the recognition of speech, with one and with two ears," *J. Acoust. Soc. Am.*, vol. 25, no. 5, pp. 975–979, 1953.
- [2] A. W. Bronkhorst, "The cocktail-party problem revisited: early processing and selection of multi-talker speech," *Atten. Percept. Psychophys.*, vol. 77, no. 5, pp. 1465–1487, Jul. 2015, doi: 10.3758/s13414-015-0882-9.
- [3] R. Plomp, "Auditory handicap of hearing impairment and the limited benefit of hearing aids," *J. Acoust. Soc. Am.*, vol. 63, no. 2, pp. 533–549, Feb. 1978, doi: 10.1121/1.381753.
- [4] E. J. Ozmeral, "The effects of hearing impairment on the ability to glimpse speech in a spectro-temporally complex noise," 2013.
- [5] E. Ceolini, I. Kiselev, and S.-C. Liu, "Evaluating Multi-Channel Multi-Device Speech Separation Algorithms in the Wild: A Hardware-Software Solution," *IEEE/ACM Trans. Audio Speech Lang. Process.*, vol. 28, pp. 1428–1439, 2020, doi: 10.1109/TASLP.2020.2989545.
- [6] I. Kiselev, E. Ceolini, D. Wong, A. De Cheveigne, and S.-C. Liu, "WHISPER: Wirelessly Synchronized Distributed Audio Sensor Platform," in *2017 IEEE 42nd Conference on Local Computer Networks Workshops (LCN Workshops)*, Oct. 2017, pp. 35–43. doi: 10.1109/LCN.Workshops.2017.62.
- [7] S. Vandecappelle, L. Deckers, N. Das, A. H. Ansari, A. Bertrand, and T. Francart, "EEG-based detection of the locus of auditory attention with convolutional neural networks," *eLife*, vol. 10, Apr. 2021, doi: 10.7554/eLife.56481.
- [8] S. Geirnaert, T. Francart, and A. Bertrand, "Riemannian geometry-based decoding of the directional focus of auditory attention using EEG," in *ICASSP 2021 - 2021 IEEE International Conference on Acoustics, Speech and Signal Processing (ICASSP)*, Jun. 2021, pp. 1115–1119. doi: 10.1109/ICASSP39728.2021.9413404.
- [9] B. Accou, J. Vanthornhout, H. V. Hamme, and T. Francart, "Decoding of the speech envelope from EEG using the VLAAl deep neural network," *Sci. Rep.*, vol. 13, no. 1, Art. no. 1, Jan. 2023, doi: 10.1038/s41598-022-27332-2.
- [10] E. Alickovic, C. F. Mendoza, A. Segar, M. Sandsten, and M. A. Skoglund, "Decoding Auditory Attention From EEG Data Using Cepstral Analysis," in *2023 IEEE International Conference on Acoustics, Speech, and Signal Processing Workshops (ICASSPW)*, Jun. 2023, pp. 1–5. doi: 10.1109/ICASSPW59220.2023.10193192.
- [11] D. Alizadeh and H. Omranpour, "EM-CSP: an efficient multiclass common spatial pattern feature method for speech imagery EEG signals recognition," *Biomed. Signal Process. Control*, vol. 84, p. 104933, Jul. 2023, doi: 10.1016/j.bspc.2023.104933.
- [12] P. Agarwal and S. Kumar, "EEG-based imagined words classification using hilbert transform and deep networks," *Multimed. Tools Appl.*, May 2023, doi: 10.1007/s11042-023-15664-8.
- [13] R. Ghosh, N. Sinha, and S. Phadikar, "Identification of imagined bengali vowels from EEG signals using activity map and convolutional neural network," in *Brain-Computer Interface*, John Wiley & Sons, Ltd, 2023, pp. 231–254. doi: 10.1002/9781119857655.ch10.
- [14] I. Kuruvila, J. Muncke, E. Fischer, and U. Hoppe, "Extracting the locus of attention at a cocktail party from single-trial EEG using a joint CNN-LSTM model," *ArXiv210203957 Cs Eess*, Feb. 2021, Accessed: Feb. 10, 2021. [Online]. Available: <http://arxiv.org/abs/2102.03957>
- [15] E. Ceolini *et al.*, "Brain-informed speech separation (BISS) for enhancement of target speaker in multitalker speech perception," *NeuroImage*, vol. 223, p. 117282, Dec. 2020, doi: 10.1016/j.neuroimage.2020.117282.
- [16] S. Geirnaert, T. Francart, and A. Bertrand, "Fast EEG-based decoding of the directional focus of auditory attention using common spatial patterns," *IEEE Trans. Biomed. Eng.*, pp. 1–1, 2020, doi: 10.1109/TBME.2020.3033446.
- [17] Y. Jiang, N. Chen, and J. Jin, "Detecting the locus of auditory attention based on the spectro-spatial-temporal analysis of EEG," *J. Neural Eng.*, vol. 19, no. 5, p. 056035, Oct. 2022, doi: 10.1088/1741-2552/ac975c.

- [18] E. Su, S. Cai, L. Xie, H. Li, and T. Schultz, "STAnet: a spatiotemporal attention network for decoding auditory spatial attention from EEG," *IEEE Trans. Biomed. Eng.*, vol. 69, no. 7, pp. 2233–2242, Jul. 2022, doi: 10.1109/TBME.2022.3140246.
- [19] S. Woo, J. Park, J.-Y. Lee, and I. S. Kweon, "CBAM: convolutional block attention module," in *Computer Vision – ECCV 2018*, V. Ferrari, M. Hebert, C. Sminchisescu, and Y. Weiss, Eds., in Lecture Notes in Computer Science, vol. 11211, 2018, pp. 3–19, doi: 10.1007/978-3-030-01234-2_1.
- [20] A. Vaswani *et al.*, "Attention is All you Need," in *Advances in Neural Information Processing Systems*, Curran Associates, Inc., 2017.
- [21] Y. Zhang, H. Ruan, Z. Yuan, H. Du, X. Gao, and J. Lu, "A learnable spatial mapping for decoding the directional focus of auditory attention using EEG," in *ICASSP 2023 - 2023 IEEE International Conference on Acoustics, Speech and Signal Processing (ICASSP)*, Jun. 2023, pp. 1–5, doi: 10.1109/ICASSP49357.2023.10096819.
- [22] Y. Ding, Y. Li, H. Sun, R. Liu, C. Tong, and C. Guan, "EEG-Deformer: A Dense Convolutional Transformer for Brain-computer Interfaces," Apr. 25, 2024, *arXiv*: arXiv:2405.00719. Accessed: May 06, 2024. [Online]. Available: <http://arxiv.org/abs/2405.00719>
- [23] M. Cai and Y. Zeng, "MAE-EEG-Transformer: A transformer-based approach combining masked autoencoder and cross-individual data augmentation pre-training for EEG classification," *Biomed. Signal Process. Control*, vol. 94, p. 106131, Aug. 2024, doi: 10.1016/j.bspc.2024.106131.
- [24] Z. He *et al.*, "Unified Convolutional Sparse Transformer for Disease Diagnosis, Monitoring, Drug Development, and Therapeutic Effect Prediction from EEG Raw Data," *Biology*, vol. 13, no. 4, Art. no. 4, Apr. 2024, doi: 10.3390/biology13040203.
- [25] X. Jin, J. Xiao, L. Jin, and X. Zhang, "Residual multimodal Transformer for expression-EEG fusion continuous emotion recognition," *CAAI Trans. Intell. Technol.*, p. cit2.12346, May 2024, doi: 10.1049/cit2.12346.
- [26] M. Liu *et al.*, "EMPT: a sparsity Transformer for EEG-based motor imagery recognition," *Front. Neurosci.*, vol. 18, Apr. 2024, doi: 10.3389/fnins.2024.1366294.
- [27] S. Geirnaert *et al.*, "Electroencephalography-based auditory attention decoding: toward neurosteered hearing devices," *IEEE Signal Process. Mag.*, vol. 38, no. 4, pp. 89–102, Jul. 2021, doi: 10.1109/MSP.2021.3075932.
- [28] Y. Yan *et al.*, "Auditory Attention Decoding in Four-Talker Environment with EEG," in *Interspeech 2024*, ISCA, Sep. 2024, pp. 432–436, doi: 10.21437/Interspeech.2024-739.
- [29] I. Rotaru, S. Geirnaert, N. Heintz, I. V. de Ryck, A. Bertrand, and T. Francart, "What are we really decoding? Unveiling biases in EEG-based decoding of the spatial focus of auditory attention," *J. Neural Eng.*, vol. 21, no. 1, p. 016017, Feb. 2024, doi: 10.1088/1741-2552/ad2214.
- [30] C. Puffay *et al.*, "Relating EEG to continuous speech using deep neural networks: a review," Feb. 06, 2023, *arXiv*: arXiv:2302.01736, doi: 10.48550/arXiv.2302.01736.
- [31] X. Xu *et al.*, "Beware of Overestimated Decoding Performance Arising from Temporal Autocorrelations in Electroencephalogram Signals," May 27, 2024, *arXiv*: arXiv:2405.17024, doi: 10.48550/arXiv.2405.17024.
- [32] L. Berthouze, L. M. James, and S. F. Farmer, "Human EEG shows long-range temporal correlations of oscillation amplitude in Theta, Alpha and Beta bands across a wide age range," *Clin. Neurophysiol.*, vol. 121, no. 8, pp. 1187–1197, Aug. 2010, doi: 10.1016/j.clinph.2010.02.163.
- [33] M. Irrmischer, S.-S. Poil, H. D. Mansvelder, F. S. Intra, and K. Linkenkaer-Hansen, "Strong long-range temporal correlations of beta/gamma oscillations are associated with poor sustained visual attention performance," *Eur. J. Neurosci.*, vol. 48, no. 8, pp. 2674–2683, 2018, doi: 10.1111/ejn.13672.
- [34] K. Linkenkaer-Hansen, V. V. Nikouline, J. M. Palva, and R. J. Ilmoniemi, "Long-Range Temporal Correlations and Scaling Behavior in Human Brain Oscillations," *J. Neurosci.*, vol. 21, no. 4, pp. 1370–1377, Feb. 2001, doi: 10.1523/JNEUROSCI.21-04-01370.2001.
- [35] V. V. Nikulin and T. Brismar, "Long-range temporal correlations in alpha and beta oscillations: effect of arousal level and test–retest reliability," *Clin. Neurophysiol.*, vol. 115, no. 8, pp. 1896–1908, Aug. 2004, doi: 10.1016/j.clinph.2004.03.019.
- [36] Y. Zhang, Z. Yuan, and J. Lu, "Auditory attention detection dataset nanjing university," Zenodo, Oct. 26, 2022, doi: 10.5281/zenodo.7253438.
- [37] C. Heunis, "Export and analysis of emotiv insight EEG data via EEGLAB." [Online]. Available: <http://rgdoi.net/10.13140/RG.2.1.3081.4326>
- [38] W. Ns, M. Gm, de W. B, I. G, and B. Na, "A validation of emotiv EPOC flex saline for EEG and ERP research," *PeerJ*. [Online]. Available: <https://pubmed.ncbi.nlm.nih.gov/32864218/>
- [39] V. Pulkki, "Virtual sound source positioning using vector base amplitude panning," *J. Audio Eng. Soc.*, vol. 45, no. 6, pp. 456–466, Jun. 1997.
- [40] S. A. Fuglsang, T. Dau, and J. Hjortkjær, "Noise-robust cortical tracking of attended speech in real-world acoustic scenes," *NeuroImage*, vol. 156, pp. 435–444, Aug. 2017, doi: 10.1016/j.neuroimage.2017.04.026.
- [41] W. Biesmans, N. Das, T. Francart, and A. Bertrand, "Auditory-inspired speech envelope extraction methods for improved EEG-based auditory attention detection in a cocktail party scenario," *IEEE Trans. Neural Syst. Rehabil. Eng.*, vol. 25, no. 5, pp. 402–412, May 2017, doi: 10.1109/TNSRE.2016.2571900.
- [42] A. Delorme and S. Makeig, "EEGLAB: an open source toolbox for analysis of single-trial EEG dynamics including independent component analysis," *J. Neurosci. Methods*, vol. 134, no. 1, pp. 9–21, Mar. 2004, doi: 10.1016/j.jneumeth.2003.10.009.

- [43] J. Capon, “High-resolution frequency-wavenumber spectrum analysis,” *Proc. IEEE*, vol. 57, no. 8, pp. 1408–1418, Aug. 1969, doi: 10.1109/PROC.1969.7278.
- [44] Y. Zhang, J. Lu, Z. Lin, F. Chen, H. Du, and X. Gao, “Electroencephalogram-based Multiclass Auditory Attention Decoding of Attended Speaker Direction,” Dec. 02, 2023, *TechRxiv*. doi: 10.36227/techrxiv.24592356.v1.
- [45] D. C. Peterson, V. Reddy, and R. N. Hamel, “Neuroanatomy, auditory pathway,” in *StatPearls*, Treasure Island (FL): StatPearls Publishing, 2022.
- [46] “PyTorch documentation — PyTorch 1.10 documentation.” [Online]. Available: <https://pytorch.org/docs/1.10/>
- [47] N. D. T. Nguyen, H. Phan, S. Geirnaert, K. Mikkelsen, and P. Kidmose, “AADNet: An End-to-End Deep Learning Model for Auditory Attention Decoding,” Oct. 16, 2024, *arXiv*: arXiv:2410.13059. Accessed: Oct. 21, 2024. [Online]. Available: <http://arxiv.org/abs/2410.13059>